

# INTERNATIONAL SOCIETY FOR SOIL MECHANICS AND GEOTECHNICAL ENGINEERING



*This paper was downloaded from the Online Library of the International Society for Soil Mechanics and Geotechnical Engineering (ISSMGE). The library is available here:*

<https://www.issmge.org/publications/online-library>

*This is an open-access database that archives thousands of papers published under the Auspices of the ISSMGE and maintained by the Innovation and Development Committee of ISSMGE.*



## SAND BEHAVIOUR UNDER STRAIN PATH CONTROL COMPORTEMENT D'UN SABLE SOUMIS A DES CHEMINS DE DEFORMATION

K. Uchida<sup>1</sup> Y.P. Vaid<sup>2</sup>

<sup>1</sup>Department of Agricultural Engineering, Kyoto University, Kyoto, Japan

<sup>2</sup>Department of Civil Engineering, University of British Columbia, Vancouver, Canada

**SYNOPSIS :** A study of sand behaviour under strain path control is presented. The advantage of strain path control is that strain uniformity in the test specimen is sustained and no shear plane is observed. This was confirmed by comparing local strain distributions calculated from the distortions of grids drawing on rubber membranes for strain path test and the conventional drained test on dense sand. Thus the validity for an element test can be extended even in the large strain domain by a positive control of strain-path. This paper describes sand behaviour under constant strain ratios of volumetric and axial strain increments, together with truly undrained and drained behaviour. It is shown that the sand behaviour under strain path control is considerably different from the behaviour under stress path control, and that true soil behavior is obtained even in the large strain domain by the positive strain path control.

### INTRODUCTION

The purpose of strain-path controlled test is to control freely the strain-path for an element test and to sustain strain uniformity in the test specimen even in the large strain domain. A special device called a *digital pressure/volume controller (DPVC)* is used for the direct strain path control. Such a device was developed and used by Olsen et al. (1988) for permeability tests on clays. Menzies (1988) introduced this device to control the triaxial test. Chu et al. (1992) recently investigated strain softening behaviour of a sand using this device, and pointed out that two types of strain softening, pre-failure and post-failure occur depending on the ratio of volumetric and axial strain increments.

In a conventional drained triaxial compression test, a shear plane is observed at large axial strain for a dense sand specimen. This causes non-uniform strain distribution within the test specimen and thus the required condition for an element test is violated. The drained volume of a medium to dense specimen first decreases, and then increases due to dilatancy. As the water flows out or into the specimen, a transient distribution of pore pressure occurs inside the specimen that accelerates non-uniform strain distribution. This has been verified by Nakamura et al. (1987) who measured strain distribution on the surface of a plane strain specimen using laser speckles method. On the other hand, for the strain-path controlled test, the distributions of pore pressure, volume change, and strain are relatively uniform because of positive control of volume change by the *DPVC* in a closed circuit of the test system. The particle sliding is considered to occur uniformly throughout the specimen, and thus strain softening may occur without development of a shear plane.

In this study, three kinds of strain-path controlled triaxial tests were conducted: (1) under constant ratios of volumetric and axial strain increment,  $d\varepsilon_v/d\varepsilon_a$ , in order to examine strain softening and deformation behaviour; (2) truly undrained triaxial test to check the quick response of corrections for membrane penetration effects; and (3) truly drained triaxial test for comparison of strain uniformity and stress-strain behaviour with those observed in the conventional drained test.

### TESTING DEVICE AND PROCEDURE

Figure 1 shows a control device for volume change, *DPVC*, interfaced

with a computer. It consists of a stepper motor and its control board, a gear box of 1/13 ratio, a ball screw and a water piston. The resolution of the stepper motor is 1.8°/step. The resolution of *DPVC* is 0.002417  $\text{cm}^3/\text{step}$ . This corresponds to  $0.60 \times 10^{-5}$  volumetric strain for the triaxial specimen (radius 6.35 cm  $\times$  height 12.70 cm). The actual resolution of *DPVC* was measured to be 0.00248  $\text{cm}^3$  ( $0.62 \times 10^{-5}$  strain) per step by a fine burette. The *DPVC* and the specimen are connected at the loading cap. This avoids interference with pore pressure measurement at the base pedestal. A back pressure of 200 kPa was always used inside the piston to maintain it deaired.

The testing material used was Ottawa sand (*ASTM Designations C-109*). Its index properties are given in Table 1. Test samples were formed by pluviating sand in deaired water, described in details by Negussey (1984). Excess sand was drawn out by a siphon for levelling the top surface. After the loading cap was in place, densification was done by tapping on the base of the triaxial cell, while maintaining the cap horizontal with the aid of a level. A vacuum of about 30 kPa was applied to the specimen as an initial confinement. After positioning the cell in the loading frame, a cell pressure of about 50 kPa was applied to change pore pressure inside the specimen from negative to positive. Then the drainage line was connected to a pore pressure transducer. The *B*-value was ensured to be greater than 0.96. Using a back pressure of 200 kPa, consolidation was allowed for about 5 minutes.

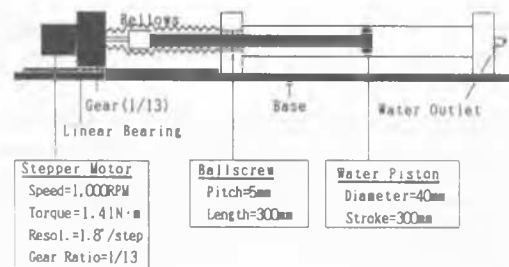


Fig. 1. digital pressure/volume controller (*DPVC*)

**Table 1. Index Properties of Ottawa Sand**

Median Particle Size	$D_{50}$ (mm)	0.39
Uniformity Coefficient	$U_c$	1.9
Specific Gravity	$G_s$	2.67
Max. Void Ratio	$e_{max}$	0.82
Min. Void Ratio	$e_{min}$	0.50
Roundness		0.60
Sphericity		0.85
Mineral Content	100%	Quartz

The drainage line was now switched to the DPVC. The strain-path controlled triaxial tests were then performed using a constant speed  $0.220 \text{ mm/min}$  for axial displacement. The end friction at both ends of specimens was substantially reduced by using anodized aluminum platens with small central stones. However, bulging of specimens was observed because the cap and pedestal had the same radii as that of the specimen.

For the constant  $d\epsilon_v/d\epsilon_a$  test, the initial hydrostatic effective confining pressures  $\sigma_3'$  used were  $100 \text{ kPa}$ ,  $200 \text{ kPa}$  and  $300 \text{ kPa}$ , and the strain increment ratios were  $-0.3$ ,  $-0.4$ ,  $-0.5$  and  $-0.7$ . The actual void ratios of specimens were in the range  $e = 0.604 - 0.635$  (average  $D_r = 60\%$ ). For the truly undrained and drained tests,  $\sigma_3'$  used was  $100 \text{ kPa}$  and there was a smaller scatter in void ratios  $e = 0.541 - 0.568$ , corresponding to a  $D_r = 80\%$ . All tests were carried out under constant radial stress. In the control program, corrections for volume change due to membrane penetration effects were applied by the method proposed by Vaid and Negussey (1984). Stresses were corrected for membrane strength as recommended by Kuerbis and Vaid (1990). Also to maintain the ratio  $d\epsilon_v/d\epsilon_a$  strictly constant, it was recognized by performing preliminary tests that the step by step feed-back operation was needed. Comparing the results with and without the feed-back operation, it was found that pore pressure at the same axial strain was larger and the peak stress was smaller for the test without the feed-back operation. For the truly undrained and drained tests, different control programs were used.

## TEST RESULTS AND DISCUSSION

### Constant $d\epsilon_v/d\epsilon_a$ Test

Figure 2 shows the test results for strain increment ratio  $d\epsilon_v/d\epsilon_a$  of  $-0.3$ ,  $-0.4$ ,  $-0.5$  and  $-0.7$ , initial effective confining pressure  $\sigma_3' = 200 \text{ kPa}$  and relative density  $D_r = 60\%$  ( $e = 0.614 - 0.635$ ). Depending upon  $d\epsilon_v/d\epsilon_a$ , two types of strain softening, pre-failure and post-failure types may be noted. The boundary between the two types being at  $d\epsilon_v/d\epsilon_a$  between the two types of softening seems to change with effective confining pressure and relative density. It is shown in Fig.2(c) that excess pore pressure increases monotonously for  $d\epsilon_v/d\epsilon_a$  (negative value) less than  $-0.5$ , but it first decreases before increasing for ratios greater than  $-0.5$ . This behaviour is interpreted as follows: when the ratio  $d\epsilon_v/d\epsilon_a$  is less than the boundary value, the speed of volume change by DPVC is in excess of the dilatancy of the specimen. Therefore, the volume change is mainly controlled by DPVC and excess pore pressure increases monotonously. This type of behaviour is similar to that of loose samples. On the other hand, when the ratio  $d\epsilon_v/d\epsilon_a$  is greater than the boundary value, the volume change is significantly controlled by the inherent dilatancy of the specimen. This type of behaviour is similar to that of dense sand.

Figure 3 presents comparison of behaviour under  $\sigma_3' = 100 \text{ kPa}$ ,  $200 \text{ kPa}$  and  $300 \text{ kPa}$  and  $d\epsilon_v/d\epsilon_a = -0.4$  and  $-0.5$ . It is seen from this figure that the stress-strain relationships and the excess pore pressure behaviour are very similar and the boundary value separating pre- and post-failure softening for  $\sigma_3' = 300 \text{ kPa}$  is estimated to be located between  $d\epsilon_v/d\epsilon_a = -0.4$  and  $-0.5$ .

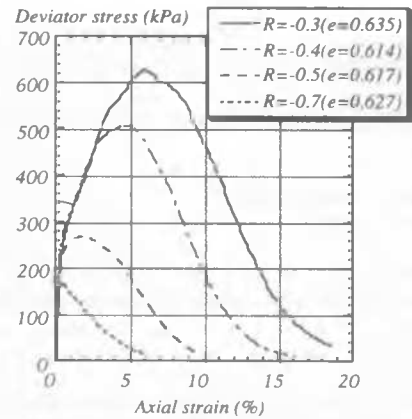


Fig.2(a)

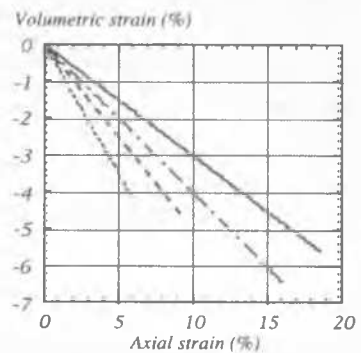


Fig.2(b)

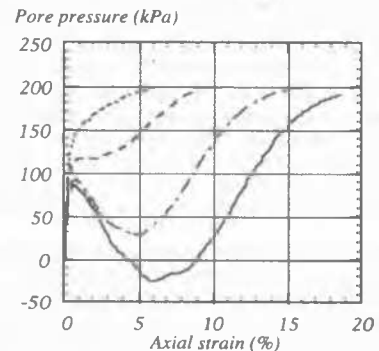


Fig.2(c)

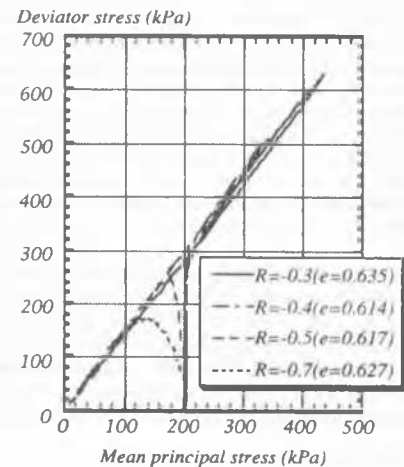


Fig.2(d)

Fig.2. Test results of constant strain increment ratio  $d\epsilon_v/d\epsilon_a$

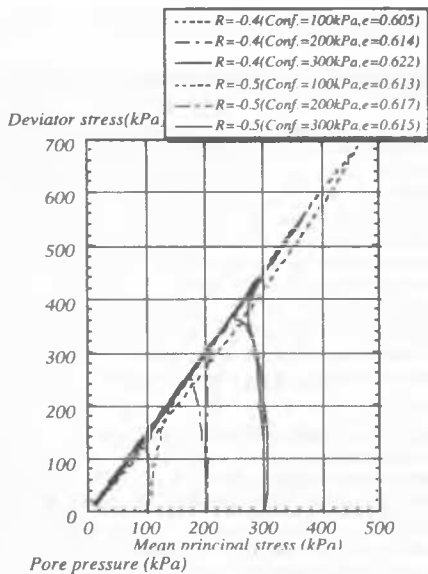


Fig.3(a)

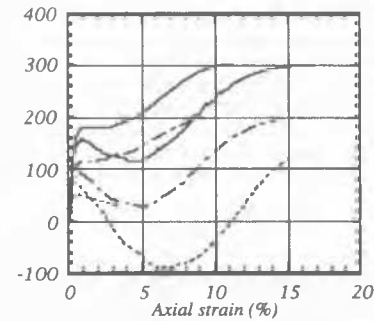


Fig.3(b)

Fig.3. Comparison of behaviour under  $\sigma_3' = 100$  kPa, 200 kPa and 300 kPa and  $d\varepsilon_v/d\varepsilon_a = -0.4$  and  $-0.5$

Figure 4 shows axial strain contours obtained from all tests with constant  $d\varepsilon_v/d\varepsilon_a$ . These contours pass through the origin and show an upward concave shape for axial strain less than 0.4% but are almost straight lines for axial strain greater than 0.5%.

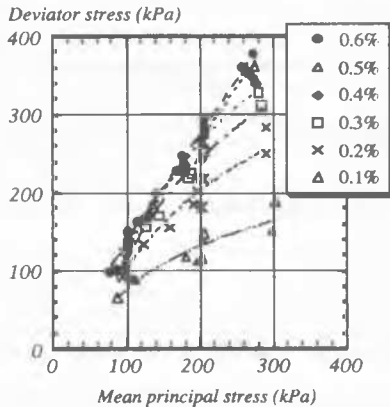


Fig.4. Axial strain contours obtained from all tests with constant  $d\varepsilon_v/d\varepsilon_a$

### Truly Undrained Test

Figure 5 shows result of a truly undrained test using the strain-path control under an initial  $\sigma_3' = 100$  kPa. The principle of this test is to make first order corrections for volume change due to membrane penetration effects using the DPVC. Tokimatsu and Nakamura (1986) proposed a membrane compensation apparatus using electropneumatic controls. Compared with this pneumatic system, the DPVC has a very quick and accurate response shown in Fig.5.

### Truly Drained Test

Figure 6 shows the results of a conventional drained test, a drained simulation test using the DPVC, and a drained test controlled under zero excess pore pressure using the DPVC. The void ratios of specimens for these tests were essentially identical,  $e = 0.562 - 0.568$ . In the drained simulation test, 159 data points obtained from the conventional drained test were used to follow the same relationship between axial strain and volumetric strain. It is noted in Fig.6(b) that the volume change behaviour in these two tests is identical as expected. In the drained test controlled under zero excess pore pressure, the feedback operation used by the DPVC was such that the pore pressure at the bottom of the specimen always agreed with the back pressure 200 kPa, Fig.6(c). It may be noted that for the conventional drained test in Fig.6(a), the deviator stress reaches a peak at an axial strain of about 2.5%, followed by a strain softening behavior. Finally, a shear plane was observed at an axial strain of about 11%.

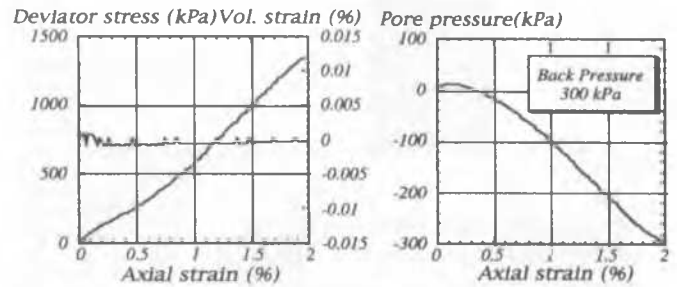


Fig.5. Result of a truly undrained test

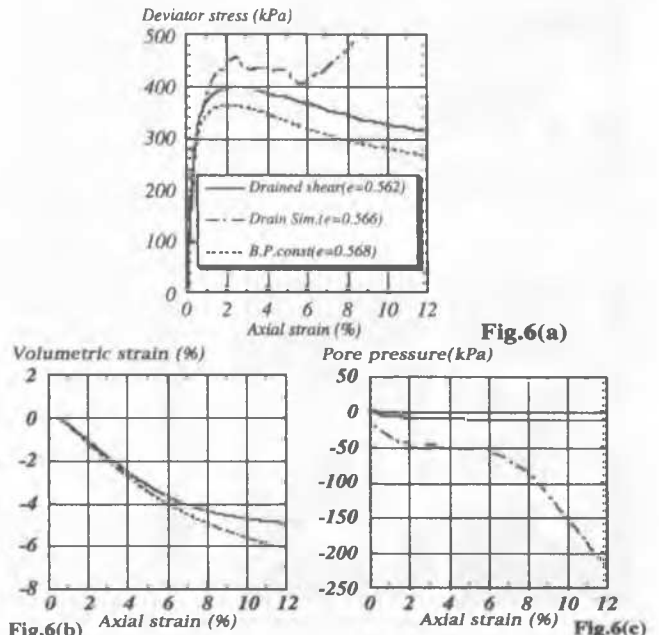


Fig.6. Results of three kinds of drained tests

excess pore pressure developed gradually in this process and reached  $-10 \text{ kPa}$  at an axial strain of about 6%. For the drained simulation test, it is noted in Fig.6(a) that the deviator stress starts increasing at an axial strain of about 6% following some strain softening. The cause of this behavior is the rapid decrease in excess pore pressure after an axial strain of about 6%, as shown in Fig.6(c). This behavior is considered to be due to strain non-uniformity in the large strain domain of these tests. On the other hand, sand behaviour in the drained test controlled under zero excess pore pressure shows significant differences in peak stress and volumetric behaviour compared to the results of other tests. No shear planes were observed in this test up to axial strain in excess of 12%. Thus, the drained test controlled under zero excess pore pressure by the DPVC can be called as the truly drained test.

Figure 7 shows the comparison between local strain distribution in the conventional drained test and the truly drained test, at an axial strain of 11%. There seem to be no significant differences between the two at an axial strain of 4%. In Fig.7, the regions of large local axial and radial strains can be identified from the upper left to lower right direction of the specimen for the conventional drained test. These areas of large local strain are consistent with the position of the shear plane observed. On the other hand, for the truly drained test, the local strain distributions are relatively uniform. Judging from the fact, it is concluded that the validity for an element test for strain uniformity can be extended even in a large strain domain if positive control of strain-path is exercised.

## CONCLUDING REMARKS

Strain-path controlled triaxial tests were performed on sand under constant strain increment ratio  $d\epsilon_v/d\epsilon_a$  as well as under truly undrained and drained conditions. The test results obtained are considerably different from the conventional stress-path controlled tests, especially with regard to strain uniformity. No shear planes were observed in strain-path controlled drained tests. In conventional drained test on dense sand, shear planes consistently appeared due to non-uniform strain distribution in the specimen. Thus the strain softening observed in the conventional test may not be a true property of the material since it is caused by non-uniformity of the strain. The strain softening observed in the strain-path controlled test is caused by particle sliding throughout the specimen and hence represents true property of the material. The two types of strain softening, pre-failure and post-failure types, were identified depending on the strain increment ratio  $d\epsilon_v/d\epsilon_a$  under constant initial  $\sigma'_1$  and  $D_r$  conditions. These two different behaviours are caused by the interrelation between DPVC and inherent dilatancy of sand contributing to volume change of the specimens. The excess pore pressure increases monotonously when DPVC controls the volume change, but it first increases and then decreases when the soil dilatancy controls. A truly undrained test can be accurately performed using the DPVC, and has a quick response compared with that obtained by the electropneumatic control device. In addition, a truly drained test can be performed under zero excess pore pressure controlled by the DPVC. This is one of the practical uses of the strain-path controlled test. By this technique the peak stress is smaller and the drained volume is larger than that in the conventional drained test. The local strain distributions for the truly drained test are more uniform than the ones for the conventional test. Therefore, it is concluded that the strain-path controlled triaxial test can yield the true soil behaviour and this test is effective for the investigation of soil behaviour in the large strain domain.

## REFERENCES

- Chu, J., Lo, S.-C.R. and Lee, I.K. (1992). Strain-softening behavior of granular soil in strain-path testing, *J. Geotech. Eng., ASCE*, Vol. 118, No. 2, pp. 191-208.
- Kuerbis, R.H. and Vaid, Y.P. (1990). Corrections for membrane strength in the triaxial test. *ASTM Geotech. Testing J.*, Vol. 13, No. 4, pp. 361-369.
- Menzies, B.K. (1988). A computer controlled hydraulic triaxial testing system, *Advanced Triaxial Testing of Soil and Rock, ASTM STP 977*, pp. 82-94.
- Nakamura, S., Tatsuoka, F. and Shin-no, F. (1987). Strain distribution in plane strain compression test of sand, *Proc. of 22th Japan National Conference on S.M.F.E.*, Vol. 1, pp. 349-352 (in Japanese).
- Negussey, D. (1984). An experimental study of small strain response of sand, *Ph.D. Thesis, The University of British Columbia, Vancouver, Canada*.
- Olsen, H.W., Morin, R.H. and Nichols, R.W. (1988). Flow pump applications in triaxial testing, *Advanced Triaxial Testing of Soil and Rock, ASTM STP 977*, pp. 68-81.
- Tokimatsu, K. and Nakamura, K. (1986). A liquefaction test without membrane penetration effects, *Soils and Foundations*, Vol. 26, No. 4, pp. 127-138.
- Vaid, Y.P. and Negussey (1984). A critical assessment of membrane penetration in triaxial test, *ASTM Geotech. Testing J.*, Vol. 7, No. 2, pp. 70-76.

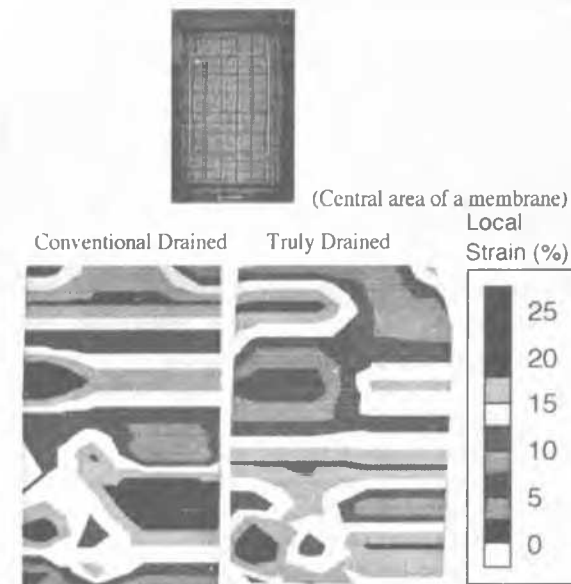


Fig.7(a). Local axial strain distribution at an axial strain of 11%

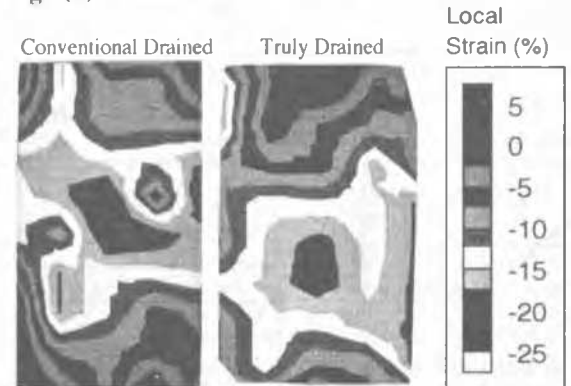


Fig.7(a). Local radial strain distribution at an axial strain of 11%

Fig.7. Comparison of local strain distributions